

Symmetry-Protected Solitons and Bulk-Boundary Correspondence in Generalized Jackiw-Rebbi Models

Chang-geun Oh¹⁺, Sang-Hoon Han²⁺, and Sangmo Cheon^{1,2,3*}

¹Research Institute for Natural Sciences, Hanyang University, Seoul, 04763, Korea

²Department of Physics, Hanyang University, Seoul, 04763, Korea

³Institute for High Pressure, Hanyang University, Seoul, 04763, Korea

⁺these authors contributed equally to this work

^{*}sangmocheon@hanyang.ac.kr

ABSTRACT

We investigate the roles of symmetry and bulk-boundary correspondence in characterizing topological edge states in generalized Jackiw-Rebbi (JR) models. We show that time-reversal (T), charge-conjugation (C), parity (P), and discrete internal field rotation (Z_n) symmetries protect and characterize the various types of edge states such as chiral and nonchiral solitons via bulk-boundary correspondence in the presence of the multiple vacua. As two representative models, we consider the JR model composed of a single fermion field having a complex mass and the generalized JR model with two massless but interacting fermion fields. The JR model shows nonchiral solitons with the Z_2 rotation symmetry, whereas it shows chiral solitons with the broken Z_2 rotation symmetry. In the generalized JR model, only nonchiral solitons can emerge with only Z_2 rotation symmetry, whereas both chiral and nonchiral solitons can exist with enhanced Z_4 rotation symmetry. Moreover, we find that the nonchiral solitons have C, P symmetries while the chiral solitons do not, which can be explained by the symmetry-invariant lines connecting degenerate vacua. Finally, we find the symmetry correspondence between multiply-degenerate global vacua and solitons such that T, C, P symmetries of a soliton inherit from global minima that are connected by the soliton, which provides a novel tool for the characterization of topological solitons.

Introduction

The bulk-boundary correspondence and symmetry play pivotal roles in understanding topological materials. The bulk-boundary correspondence is that those of the bulk govern the topological properties of the edge modes, and it has been confirmed in many topological materials^{1,2}. Symmetry classifies and protects the topological properties of such materials. For instance, topological insulators and superconductors are classified by 10-fold Altland-Zirnbauer classes³⁻⁵, based on time-reversal (T), charge-conjugation (C), and chiral symmetries, and topological crystalline insulators are protected by space-group symmetries⁶⁻⁹. These studies strongly imply that analyzing the bulk and symmetry is important to understand the physical properties of topological edge states.

The Jackiw-Rebbi (JR) and Su-Schrieffer-Heeger (SSH) models are the famous 1D models presenting such topological behaviour¹⁰⁻¹⁵. The JR model describes a massless fermion field interacting with a nontrivial soliton background bose field in one spatial dimension¹⁰⁻¹². These models exhibit soliton's exotic topological properties such as zero-energy mode, a half fermion number, and spin-charge separation only when the nontrivial topology of bulk is protected by either C or parity (P) symmetry. This pioneering study is an example of the general principle that symmetry leads to richer topology and has stimulated many studies: conducting polymer¹⁴, diatomic chain¹⁶, magnetic system¹⁷, photonic crystal systems¹⁸⁻²⁰, artificially engineered SSH lattices^{21,22}, ultracold atomic systems²³⁻²⁷ and so on. Though there were several attempts to extend the SSH and JR models^{16,28-38}, there have been only a few limited studies about the roles of symmetry and bulk-boundary correspondence that distinguish the nature of topological solitons beyond the SSH and JR models.

Chiral edge states are ubiquitous in nature and often protected by topology and symmetry^{1,2,39}. Such chiral topological excitations are expected to show promise for information technology due to their robustness against external perturbations⁴⁰⁻⁴², and had been treated as the hallmark of 2D and 3D topological insulators^{1,2}. Recently, topological solitons having chirality or chiral solitons were experimentally realized in a 1D electronic system with Z_4 topological symmetry^{35,43}. Chiral switching using such solitons was demonstrated, which implies that chiral and nonchiral solitons are expected to be used as multi-digit information carriers⁴⁴. However, the universal conditions for the emergence of chiral and nonchiral solitons in 1D are not disclosed yet.

The purpose of this Letter is to discover the role of symmetry and bulk-boundary correspondence in characterizing various topological solitons in 1D systems using JR models. In this work, we show that the cooperation of time-reversal, charge-conjugation, parity, and discrete field rotation (Z_n) symmetries protects and identifies the various types of soliton states via bulk-boundary correspondence. We consider two representative models: The JR model, composed of a single fermion field with a complex mass, possesses phase rotation symmetry. The generalized JR model with two massless but interacting fermion fields has a discrete internal field rotation symmetry. The JR model shows charge-conjugate and parity-invariant solitons (equivalently, nonchiral solitons) in the presence of Z_2 field rotation symmetry, otherwise it shows chiral solitons with broken C and P symmetries. The generalized JR model allows more abundant kinds of solitons—nonchiral (NC), right chiral (RC), and left chiral (LC) solitons [Fig. 2(d)]—depending on the controllable physical parameters. In the generalized JR model, the Z_2 rotation symmetry protects NC solitons imposing the equivalence between an NC soliton and its anti-NC soliton. The enhanced Z_4 rotation symmetry promotes the symmetry of global minima from Z_2 to Z_4 , which endows the chirality to solitons. Therefore, we reveal that the internal symmetry enriches the variety of topological solitons in 1D systems. Further T , C , P analysis discloses that a pair of chiral solitons forms a particle-antiparticle pair, while a nonchiral soliton is its antiparticle. Finally, we discover the symmetry correspondence between multiply-degenerate global vacua and solitons such that T , C , P symmetries of a soliton inherit from global minima that are connected by the soliton.

Results and Discussion

The low-energy effective theory of the SSH ($m_z = 0$) and the Rice-Mele (RM, $m_z \neq 0$) models^{15,16} is described by the Lagrangian density of the JR model¹² with a fermion mass m_z [Fig. 1(a,b)]:

$$\mathcal{L}_{\text{JR}} = \bar{\psi}[i\gamma^0\partial_0 + i\gamma^1\partial_1 - \phi(x) - i\gamma^5 m_z]\psi, \quad (1)$$

where $\psi(x)$ and $\phi(x)$ are two-component spinor and bose fields, and $\gamma^0 = \sigma^y$, $\gamma^1 = -i\sigma^z$, $\gamma^5 = \sigma^x$. The mass terms can be represented as $\phi(x) + i\gamma^5 m_z = m(x)e^{i\gamma^5\theta(x)}$, where $m(x) = \sqrt{\phi^2(x) + m_z^2}$ and $\tan\theta(x) = \frac{m_z}{\phi(x)}$. For a homogeneous bose field, $\phi(x) = \phi_0$, this model has gapped spectra of $E = \pm\sqrt{k_x^2 + \phi_0^2 + m_z^2}$ and two degenerate vacua. In the complex plane, the two degenerate vacua are located at θ and $\pi - \theta$ with $\tan\theta = \frac{m_z}{\phi_0}$, which are denoted as A and B (A' and B') for the SSH (RM) model [Fig. 1(c)]. If the bose field $\phi(x)$ becomes a solitonic background field, $\phi(x) = \phi_s(x)$, that interpolates the two degenerate vacua, there appears an isolated soliton mode in the gap. Depending on m_z , the emergent soliton modes are different. The soliton modes in the SSH model are zero-energy modes, while the RM type soliton modes are not [Fig. 1(a,b)].

The JR model in Eq. (1) has the following global rotation symmetry:

$$\theta \rightarrow \theta + \tilde{\theta}, \quad \psi(t, x) \rightarrow U\psi = i\exp\left(-i\gamma^5\frac{\tilde{\theta}}{2}\right)\psi(t, x). \quad (2)$$

Because we are interested in the rotation symmetry that exchanges the two global minima, we set $\tilde{\theta} = \pi - 2\theta$. The rotation symmetry in Eq. (2) becomes Z_2 symmetry (equivalently, π symmetry) only when $\theta = 0$ (or $m_z = 0$):

$$\phi(x) \rightarrow e^{i\pi}\phi(x), \quad \psi(t, x) \rightarrow \gamma^5\psi(t, x). \quad (3)$$

We also analyze T , C , and P symmetries. Because the JR model is spinless, T symmetry exists. On the other hand, the Lagrangian density in Eq. (1) has C and P symmetries only when $m_z = 0$:

$$C\psi(t, x)C^{-1} = \psi^*(t, x), \quad (4)$$

$$P\psi(t, x)P^{-1} = \gamma^0\psi(t, -x), \quad P\phi(x)P^{-1} = \phi(-x). \quad (5)$$

Therefore, Z_2 rotation (or π rotation) symmetry protects the C and P symmetries, and vice versa. Moreover, when the bose field is a soliton field, $\phi(x) = \phi_s(x)$, the soliton system—composed of $\psi_s(x)$ and $\phi_s(x)$ —is self-charge conjugate and parity-invariant^{10–12}. Thus, the JR model shows charge-conjugate and parity-invariant solitons (or, equivalently, nonchiral solitons) in the presence of the enhanced Z_2 rotation symmetry, otherwise it shows chiral solitons with broken C and P symmetries.

The solitons in the JR model can also be distinguished by topology. With T , C , P and Z_2 symmetries, the two minima in the JR model are distinguished by their quantized Berry phases; hence, the topological phase transition between the two minima occurs through the SSH type soliton. With broken C , P , and Z_2 symmetries, in the RM model, the topology of the two minima can be continuously connected due to the fermion mass; thus, the soliton does not involve such phase transitions. Thus, an enhanced rotation symmetry can endow richer topological structures to solitons [Fig. 1(d)].

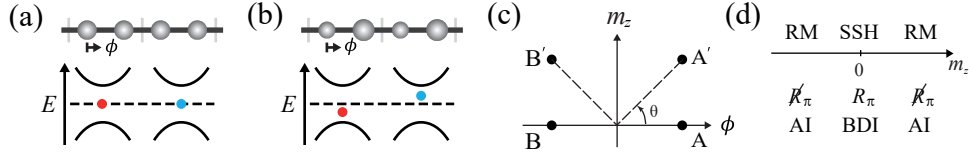


Figure 1. Schematics of atom configurations and band structures for (a) SSH and (b) RM models. ϕ is a dimerization displacement that corresponds to a bose field $\phi(x)$ in JR model. Red and blue circles represent isolated soliton and antisoliton modes in the gap, respectively. (c) The degenerate vacua for SSH and RM models in the order parameter space of (ϕ, m_z) : A and B (A' and B') for the SSH (RM) model. (d) Atland-Zirnbauer class³ and π rotation symmetry with respect to the fermion mass m_z . R_π (\cancel{R}_π) indicates that the π rotation symmetry is preserved (broken).

Now, we consider the generalized JR model composed of two massless fermion fields and two interfield couplings (t_1, t_2) . The Lagrangian density is given by

$$\mathcal{L} = \mathcal{L}_1 + \mathcal{L}_2 + \mathcal{L}_B + \mathcal{L}_{\text{int}}, \quad (6)$$

$$\mathcal{L}_j = \bar{\Psi}_j [i\partial - \Phi_j] \Psi_j, \quad \mathcal{L}_B = -\frac{K}{2} (\Phi_1^2 + \Phi_2^2), \quad (7)$$

$$\mathcal{L}_{\text{int}} = -\bar{\Psi}_1 [t_1 \gamma^0 - it_2 \gamma^1] \Psi_2 - \bar{\Psi}_2 [t_1 \gamma^0 + it_2 \gamma^1] \Psi_1, \quad (8)$$

where Ψ_j and Φ_j are a two-component spinor field and a real scalar bose field localized in the j -th wire ($j = 1, 2$), respectively. \mathcal{L}_B corresponds to the potential of the bose fields, and K is a positive constant. Figure 2 shows a schematic, the total energy profile, and solitons for several t_2/t_1 values. When $t_1 \neq t_2$, there are two global and two local energy minima, and the atomic configuration in a global minimum has a staggered dimerization ordering. As a realistic example, this case can describe the low-energy effective theory of the quasi-1D systems of polyacetylene chains^{45–47}. At the critical point $t_1 = t_2$, the two local minima transform to global minima resulting in Z_4 symmetric four degenerate global minima. For example, this case can describe the low-energy effective theory of the coupled double Peierls chain model and explains the charge density wave system of indium atomic wires^{35,48,49}. The generalized JR model allows various kinds of solitons depending on t_1 and t_2 . When $t_1 \neq t_2$, only nonchiral solitons can exist, whereas chiral solitons can additionally exist at the critical point ($t_1 = t_2$), as shown in Fig. 2(d). The nature of chiral and nonchiral solitons will be explained shortly.

We find that the enhanced Z_4 rotation symmetry supports the emergence of chiral and nonchiral solitons. Using Clifford matrices, the Lagrangian density in Eq. (6) can be rewritten as follows:

$$\mathcal{L} = \bar{\Psi} [\Gamma_2 i \partial_0 + \Gamma_3 \partial_1 + t_1 \Gamma_{34} - it_2 \Gamma_{25} - \Phi] \Psi + \mathcal{L}_B, \quad (9)$$

where $\Psi = (\Psi_1, \Psi_2)$, $\Phi = \begin{pmatrix} \Phi_1 & 0 \\ 0 & \Phi_2 \end{pmatrix}$, $\bar{\Psi} = \Psi^\dagger \Gamma_2$ and the form of Clifford matrices Γ_i are given in Sec. S2.1. in Supplemental Information. Depending on interfield couplings, this Lagrangian density can have Z_2 rotation symmetry ($n = 2$; π rotation symmetry) or Z_4 rotation symmetry ($n = 1$; $\pi/2$ rotation symmetry):

$$\Psi(t, x) \rightarrow \begin{pmatrix} 0 & -i\sigma_x \\ 1 & 0 \end{pmatrix}^n \Psi(t, x), \quad (10)$$

$$\Phi(x) \rightarrow e^{i\Gamma_{14}\theta} \Phi(x), \quad (11)$$

where $e^{i\Gamma_{14}\theta} = \begin{pmatrix} \cos \theta & \sin \theta \\ -\sin \theta & \cos \theta \end{pmatrix}$ and $\theta = \frac{n\pi}{2}$. Similar to the JR model, the Z_2 rotation exchanges two global minima that are located oppositely with respect to the origin in order parameter space [Fig. 2(b)]. Hence, the Z_2 rotation symmetry implies that an NC soliton and its anti-NC soliton systems are identical, which indicates that the Lagrangian for an NC soliton system satisfies C and P symmetries as discussed later. While the action is invariant under the Z_2 rotation regardless of t_1 and t_2 , the Z_4 rotation symmetry is realized only at the critical point $t_1 = t_2$ [Sec. S2.6. in Supplementary Information]. The Z_4 rotation rotates the energy profile counterclockwise by $\pi/2$ and hence the Z_4 symmetry guarantees four degenerate global minima, which indicates that the Z_4 rotation symmetry is necessary for the simultaneous emergence of the chiral and nonchiral solitons. In addition, the Z_4 rotation symmetry supports the equivalence relations among the same type of solitons because it changes a soliton to the soliton rotated counterclockwise by the same angle in order parameter space [Fig. 2(d)].

We analyze T , C , P symmetries in the generalized JR model [see details in Sec. S2.5 of Supplementary Information]. T symmetry is always present as the JR model is spinless. On the other hand, C and P symmetries exist only along with the

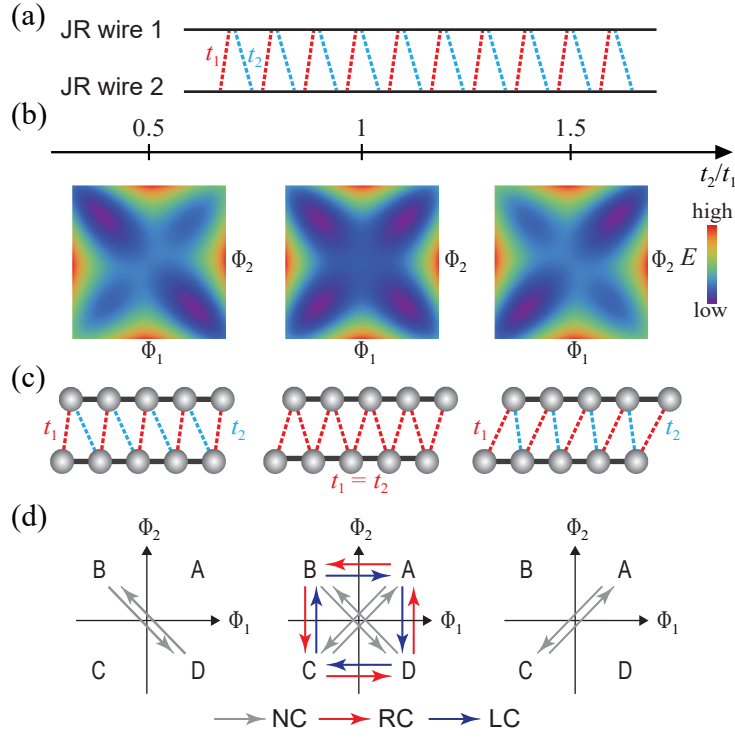


Figure 2. (a) Schematic for the generalized JR model composed of two JR wires and two interwire couplings (t_1 and t_2). In each i th JR wire, the i th fermion and bose fields, $\Psi_i(t, x)$ and $\Phi_i(t, x)$, reside. (b) Total energy profiles, (c) the corresponding lattice models, and (d) diagrams of possible solitons in the order parameter space (Φ_1, Φ_2) for three t_2/t_1 values. In (d), nonchiral (NC), right chiral (RC), and left chiral (LC) solitons are represented by grey, red and blue arrows, respectively. A, B, C, and D indicate global and local minima.

symmetry-invariant lines (AC and BD lines), and their forms are different depending on the lines [Fig. 3(b)]. The Lagrangian density in Eq. (9) has the following symmetries: For the AC line,

$$C\Psi(t, x)C^{-1} = -\Gamma_{14}\Psi^*(t, x), \quad (12)$$

$$P\Psi(t, x)P^{-1} = \Gamma_{34}\Psi(t, -x), \quad (13)$$

and for the BD line,

$$C\Psi(t, x)C^{-1} = -\Gamma_5\Psi^*(t, x), \quad (14)$$

$$P\Psi(t, x)P^{-1} = \Gamma_{24}\Psi(t, -x). \quad (15)$$

In the viewpoint of energetics, only one symmetry-invariant line is realized when $t_1 \neq t_2$, whereas both symmetry-invariant lines are realized at the critical point $t_1 = t_2$. This indicates that the Z_4 rotation symmetry gives the coexistence of the two symmetry-invariant lines.

Now we unveil the symmetries of soliton systems by explicitly analyzing the Lagrangian density for soliton systems [see details in Sec. S2.5 of Supplementary Information]. An NC soliton system has T, C, P symmetries because the bose fields are localized in the symmetry-invariant line (AC or BD line). This indicates that an AC soliton is its antiparticle having no chirality. On the other hand, in RC and LC soliton systems, C and P symmetries are broken because the bose fields deviate from the symmetry-invariant line, which naturally endows the chirality to solitons. However, the charge conjugated and parity transformed fields of an RC soliton system can be described by the fields of an LC soliton system, and vice versa:

$$C\Psi_{RC(i \rightarrow j)}(t, x)C^{-1} = -\Gamma_{14}U\Psi_{LC(j \rightarrow i)}^*(t, x), \quad (16)$$

$$P\Psi_{RC(i \rightarrow j)}(t, x)P^{-1} = \Gamma_{34}U^*\Psi_{LC(j \rightarrow i)}(t, -x), \quad (17)$$

where i and j in the subscript indicate two global minima that the corresponding soliton field connects, and the unitary matrices

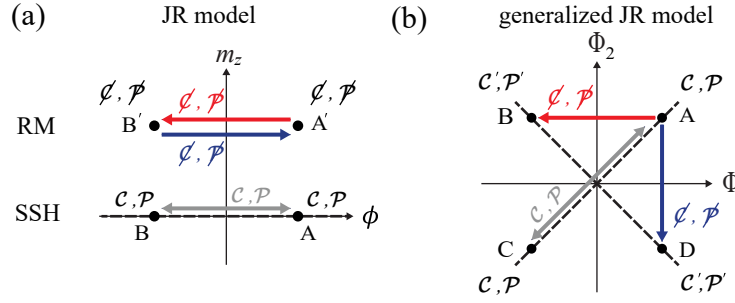


Figure 3. Diagrams for C and P symmetries of global minima and solitons for the (a) JR and (b) generalized JR models. C and P indicate the symmetries, while \mathcal{C} and \mathcal{P} do broken symmetries. The dashed lines represent C and P symmetry-invariant lines. In (a), the ϕ axis and the symmetry-invariant line are overlapped. The gray arrow represents solitons in the SSH model, and red and blue arrows do in the RM model. A and B (A' and B') are two degenerate vacua for the SSH (RM) model. In (b), the prime in superscript represents that the corresponding symmetry transformation has a different form comparing with the unprimed one. The red, blue, and gray arrows represent right-chiral, left-chiral, and non-chiral solitons, respectively.

U are given by

$$U = \begin{pmatrix} 0 & 1 \\ -i\sigma_x & 0 \end{pmatrix}, \quad \text{when } (i, j) = (A, B) \text{ or } (C, D),$$

$$U = \begin{pmatrix} 0 & i\sigma_x \\ 1 & 0 \end{pmatrix}, \quad \text{when } (i, j) = (B, C) \text{ or } (D, A).$$

This indicates that the RC and LC solitons are charge-conjugate and parity partner, i.e., they satisfy particle-antiparticle duality. Similarly, in the JR model, particle-antiparticle duality between soliton and antisoliton can be proved [Sec. S1.4. in Supplementary Information].

Similar to the bulk-boundary correspondence in topological insulators, we discover symmetry correspondences between multiple global minima and various types of solitons. T , C , P symmetries of a soliton are determined by the symmetries of two global minima connected by the soliton. Thus, the symmetry properties of solitons can be obtained without definitive proof for the soliton system. Figure 3 shows the diagrams of T , C , P symmetries for the JR and generalized JR models. In the SSH soliton system, two global minima are located in a symmetry-invariant line, and hence both two global minima and solitons connecting them have T , C , P symmetries. In the RM soliton system, two global minima do not have C and P symmetries, hence the solitons do not have C and P symmetries. In the generalized JR model with the Z_4 rotation symmetry, each global minima have T , C and P symmetries. However, the forms of C and P transformations are different according to the symmetry-invariant AC or BD lines, as discussed before. When a soliton interpolates two global minima in the AC or BD line, the soliton has T , C , P symmetries, which results in a self-charge-conjugated and parity-invariant NC soliton. When a soliton connects two global minima out of the same symmetry-invariant line, the soliton does not have C and P symmetries, which endows chirality to the RC and LC solitons as shown in Fig. 3(b).

Such C duality between chiral soliton systems and C symmetry in a non-chiral soliton system appear in physical observables such as energy spectra and fermion numbers of isolated soliton modes. In the generalized JR model, two isolated soliton modes for each soliton system appear, and they are the results of fractionalization or hybridization of zero modes [Fig. 4]. For RC and LC soliton systems, one isolated energy mode is the primary mode, and the other is the induced mode [Fig. 4(a,b)]. When a soliton field exists in one fermion field resulting in the primary mode, an effective soliton field is induced in the other fermion field due to the interfield couplings, which leads to the emergence of the induced mode. Thus, a zero mode is fractionalized into primary and induced modes. For an NC soliton system, the two isolated energy modes are distinguishable as bonding and antibonding modes regardless of t_1 and t_2 when $t_1 t_2 \neq 0$ [Fig. 4(c)]. They are the result of hybridization between two zero modes.

We calculate the energy spectra and fermion numbers of such isolated soliton modes using the effective one-particle Hamiltonian and Goldstone-Wilczek method⁵⁰. See detailed calculations in Sec. S2. of Supplemental Information. Figure 4(d-f) shows the energy spectra with respect to the strength of the interwire coupling at the critical point ($t_1 = t_2$). The bonding and antibonding modes in an NC soliton system are symmetrically located with respect to $E = 0$ because of C symmetry [Fig. 4(f)]. Because the nature of an NC soliton is protected by the Z_2 rotation symmetry and symmetry-invariant lines, the symmetric spectra of an NC soliton are maintained even if $t_1 \neq t_2$ [see Fig. S1 in Supplementary Information]. However, primary and induced modes in each RC and LC soliton system are not symmetrically located because C symmetry is broken. Instead, the

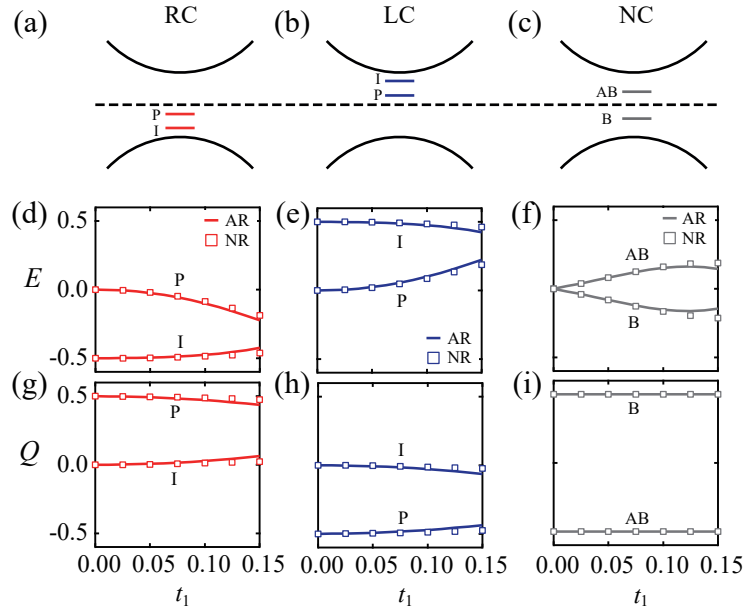


Figure 4. Schematics for the soliton modes of (a) RC, (b) LC, and (c) NC soliton systems. Energy spectra for soliton modes for (d) RC, (e) LC, and (f) NC systems with respect to t_1 . The spectra are normalized by the energy gap for each t_1 . The fermion numbers for soliton modes with respect to t_1 for (g) RC, (h) LC, and (i) NC systems. P, I, AB, and B represent the primary, induced, antibonding, and bonding modes, respectively. Analytical results (AR; lines) and numerical results (NR; squares) are calculated at the critical point $t_1 = t_2$.

isolated energy modes in the RC soliton system are located symmetrically with the isolated energy modes in the LC soliton system [Fig. 4(d,e)]. This indicates that the RC and LC solitons form a charge-conjugate pair and satisfy C duality. Figure 4(g-i) shows the fermion number of each isolated mode with respect to the strength of the interfield coupling. We now consider the Fermi-level at $E = 0$, i.e., the bonding mode in an NC soliton system and soliton modes in an RC soliton system are filled, while the other modes are empty. Similar to the energy spectra of RC and LC solitons, the fermion numbers of RC and LC solitons are also opposite [Fig. 4(g,h)]. The fermion number for the bonding and antibonding modes in an NC soliton system are also oppositely positioned, as shown in Fig. 4(i). This behavior is maintained even for $t_1 \neq t_2$ case [see Sec. S2.3. in Supplementary Information]. Similarly, for the JR model, the spectra of isolated soliton and antisoliton modes show the C duality and C symmetry [Fig. 1(a,b)]. Therefore, chiral soliton shows C duality, while nonchiral solitons do C symmetry.

Conclusion

In summary, we have studied the roles of symmetry and bulk-boundary correspondence in the JR and generalized JR models. We showed that the cooperation between T , C , P , and internal discrete field rotation symmetries characterizes the physical properties of topological solitons in 1D systems. Furthermore, we found bulk-boundary correspondence between the multiply degenerate global minima and solitons such that the symmetry of a soliton inherits the symmetries of two global minima that the soliton interpolates. Our work can be generally applied to 1D systems such as conducting polymers⁵¹, charge density wave systems⁵², engineered atomic chain systems²¹, photonic crystal systems⁵³, ultracold atomic systems⁵⁴, and higher dimensional systems.

References

1. Hasan, M. Z. & Kane, C. L. *Colloquium* : Topological insulators. *Rev. Mod. Phys.* **82**, 3045–3067, DOI: [10.1103/RevModPhys.82.3045](https://doi.org/10.1103/RevModPhys.82.3045) (2010).
2. Qi, X.-L. & Zhang, S.-C. Topological insulators and superconductors. *Rev. Mod. Phys.* **83**, 1057–1110, DOI: [10.1103/RevModPhys.83.1057](https://doi.org/10.1103/RevModPhys.83.1057) (2011).
3. Altland, A. & Zirnbauer, M. R. Nonstandard symmetry classes in mesoscopic normal-superconducting hybrid structures. *Phys. Rev. B* **55**, 1142–1161, DOI: [10.1103/PhysRevB.55.1142](https://doi.org/10.1103/PhysRevB.55.1142) (1997).

4. Schnyder, A. P., Ryu, S., Furusaki, A. & Ludwig, A. W. W. Classification of topological insulators and superconductors in three spatial dimensions. *Phys. Rev. B* **78**, 195125, DOI: [10.1103/PhysRevB.78.195125](https://doi.org/10.1103/PhysRevB.78.195125) (2008).
5. Ryu, S., Schnyder, A. P., Furusaki, A. & Ludwig, A. W. W. Topological insulators and superconductors: tenfold way and dimensional hierarchy. *New J. Phys.* **12**, 065010, DOI: [10.1088/1367-2630/12/6/065010](https://doi.org/10.1088/1367-2630/12/6/065010) (2010).
6. Ando, Y. & Fu, L. Topological Crystalline Insulators and Topological Superconductors: From Concepts to Materials. *Annu. Rev. Condens. Matter Phys.* **6**, 361–381, DOI: [10.1146/annurev-conmatphys-031214-014501](https://doi.org/10.1146/annurev-conmatphys-031214-014501) (2015).
7. Hsieh, T. H. *et al.* Topological crystalline insulators in the SnTe material class. *Nat Commun* **3**, 982, DOI: [10.1038/ncomms1969](https://doi.org/10.1038/ncomms1969) (2012).
8. Fang, C. & Fu, L. New classes of three-dimensional topological crystalline insulators: Nonsymmorphic and magnetic. *Phys. Rev. B* **91**, 161105(R), DOI: [10.1103/PhysRevB.91.161105](https://doi.org/10.1103/PhysRevB.91.161105) (2015).
9. Fu, L. Topological Crystalline Insulators. *Phys. Rev. Lett.* **106**, 106802, DOI: [10.1103/PhysRevLett.106.106802](https://doi.org/10.1103/PhysRevLett.106.106802) (2011).
10. Jackiw, R. & Semenoff, G. Continuum quantum field theory for a linearly conjugated diatomic polymer with fermion fractionization. *Phys. Rev. Lett.* **50**, 439–442, DOI: [10.1103/PhysRevLett.50.439](https://doi.org/10.1103/PhysRevLett.50.439) (1983).
11. Jackiw, R. & Schrieffer, J. Solitons with fermion number in condensed matter and relativistic field theories. *Nucl. Phys. B* **190**, 253–265, DOI: [10.1016/0550-3213\(81\)90557-5](https://doi.org/10.1016/0550-3213(81)90557-5) (1981).
12. Jackiw, R. & Rebbi, C. Solitons with fermion number $\frac{1}{2}$. *Phys. Rev. D* **13**, 3398–3409, DOI: [10.1103/PhysRevD.13.3398](https://doi.org/10.1103/PhysRevD.13.3398) (1976).
13. Niemi, A. & Semenoff, G. Fermion number fractionization in quantum field theory. *Phys. Reports* **135**, 99–193, DOI: [10.1016/0370-1573\(86\)90167-5](https://doi.org/10.1016/0370-1573(86)90167-5) (1986).
14. Heeger, A. J., Kivelson, S., Schrieffer, J. R. & Su, W. P. Solitons in conducting polymers. *Rev. Mod. Phys.* **60**, 781–850, DOI: [10.1103/RevModPhys.60.781](https://doi.org/10.1103/RevModPhys.60.781) (1988).
15. Su, W. P., Schrieffer, J. R. & Heeger, A. J. Solitons in Polyacetylene. *Phys. Rev. Lett.* **42**, 1698–1701, DOI: [10.1103/PhysRevLett.42.1698](https://doi.org/10.1103/PhysRevLett.42.1698) (1979).
16. Rice, M. J. & Mele, E. J. Elementary Excitations of a Linearly Conjugated Diatomic Polymer. *Phys. Rev. Lett.* **49**, 1455–1459, DOI: [10.1103/PhysRevLett.49.1455](https://doi.org/10.1103/PhysRevLett.49.1455) (1982).
17. Bluhm, H. *et al.* Dephasing time of GaAs electron-spin qubits coupled to a nuclear bath exceeding 200 μ s. *Nat. Phys* **7**, 109–113, DOI: [10.1038/nphys1856](https://doi.org/10.1038/nphys1856) (2011).
18. Zhou, X.-F. *et al.* Dynamically Manipulating Topological Physics and Edge Modes in a Single Degenerate Optical Cavity. *Phys. Rev. Lett.* **118**, 083603, DOI: [10.1103/PhysRevLett.118.083603](https://doi.org/10.1103/PhysRevLett.118.083603) (2017).
19. Zhao, H. *et al.* Topological hybrid silicon microlasers. *Nat Commun* **9**, 981, DOI: [10.1038/s41467-018-03434-2](https://doi.org/10.1038/s41467-018-03434-2) (2018).
20. St-Jean, P. *et al.* Lasing in topological edge states of a one-dimensional lattice. *Nat. Photon* **11**, 651–656, DOI: [10.1038/s41566-017-0006-2](https://doi.org/10.1038/s41566-017-0006-2) (2017).
21. Huda, M. N., Kezilebieke, S., Ojanen, T., Drost, R. & Liljeroth, P. Tuneable topological domain wall states in engineered atomic chains. *npj Quantum Mater.* **5**, 17, DOI: [10.1038/s41535-020-0219-3](https://doi.org/10.1038/s41535-020-0219-3) (2020).
22. Queraltó, G. *et al.* Topological state engineering via supersymmetric transformations. *Commun Phys* **3**, 49, DOI: [10.1038/s42005-020-0316-4](https://doi.org/10.1038/s42005-020-0316-4) (2020).
23. Atala, M. *et al.* Direct measurement of the zak phase in topological bloch bands. *Nat. Phys.* **9**, 795–800 (2013).
24. Nakajima, S. *et al.* Topological thouless pumping of ultracold fermions. *Nat. Phys.* **12**, 296–300 (2016).
25. Lu, H.-I. *et al.* Geometrical pumping with a bose-einstein condensate. *Phys. review letters* **116**, 200402 (2016).
26. Leder, M. *et al.* Real-space imaging of a topologically protected edge state with ultracold atoms in an amplitude-chirped optical lattice. *Nat. communications* **7**, 1–8 (2016).
27. Meier, E. J., An, F. A. & Gadway, B. Observation of the topological soliton state in the su–schrieffer–heeger model. *Nat. communications* **7**, 1–6 (2016).
28. Väyrynen, J. I. & Ojanen, T. Chiral topological phases and fractional domain wall excitations in one-dimensional chains and wires. *Phys. Rev. Lett.* **107**, 166804 (2011).
29. Li, L., Xu, Z. & Chen, S. Topological phases of generalized Su-Schrieffer-Heeger models. *Phys. Rev. B* **89**, 085111 (2014).

30. Shiozaki, K., Sato, M. & Gomi, K. Z_2 topology in nonsymmorphic crystalline insulators: Möbius twist in surface states. *Phys. Rev. B* **91**, 155120 (2015).
31. Zhao, Y. X. & Schnyder, A. P. Nonsymmorphic symmetry-required band crossings in topological semimetals. *Phys. Rev. B* **94**, 195109 (2016).
32. Zhang, S.-L. & Zhou, Q. Two-leg Su-Schrieffer-Heeger chain with glide reflection symmetry. *Phys. Rev. A* **95**, 061601(R) (2017).
33. Velasco, C. G. & Paredes, B. Realizing and Detecting a Topological Insulator in the AIII Symmetry Class. *Phys. Rev. Lett.* **119**, 115301 (2017).
34. Xie, D., Gou, W., Xiao, T., Gadway, B. & Yan, B. Topological characterizations of an extended Su–Schrieffer–Heeger model. *npj Quantum Inf.* **5**, 1–5 (2019).
35. Cheon, S., Kim, T.-H., Lee, S.-H. & Yeom, H. W. Chiral solitons in a coupled double Peierls chain. *Science* **350**, 182–185, DOI: [10.1126/science.aaa7055](https://doi.org/10.1126/science.aaa7055) (2015).
36. Han, S.-H., Jeong, S.-G., Kim, S.-W., Kim, T.-H. & Cheon, S. Topological features of ground states and topological solitons in generalized Su-Schrieffer-Heeger models using generalized time-reversal, particle-hole, and chiral symmetries. *Phys. Rev. B* **102**, 235411, DOI: [10.1103/PhysRevB.102.235411](https://doi.org/10.1103/PhysRevB.102.235411) (2020).
37. Oh, C.-g., Han, S.-H., Jeong, S.-G., Kim, T.-H. & Cheon, S. Particle-antiparticle duality and fractionalization of topological chiral solitons. *Sci Rep* **11**, 1013, DOI: [10.1038/s41598-020-80085-8](https://doi.org/10.1038/s41598-020-80085-8) (2021).
38. Go, G., Kang, K. T. & Han, J. H. Solitons in one-dimensional three-band model with a central flat band. *Phys. Rev. B* **88**, 245124, DOI: [10.1103/PhysRevB.88.245124](https://doi.org/10.1103/PhysRevB.88.245124) (2013).
39. Chiu, C.-K., Teo, J. C. Y., Schnyder, A. P. & Ryu, S. Classification of topological quantum matter with symmetries. *Rev. Mod. Phys.* **88**, 035005, DOI: [10.1103/RevModPhys.88.035005](https://doi.org/10.1103/RevModPhys.88.035005) (2016). ArXiv: 1505.03535.
40. Braun, H.-B. Topological effects in nanomagnetism: from superparamagnetism to chiral quantum solitons. *Adv. Phys.* **61**, 1–116, DOI: [10.1080/00018732.2012.663070](https://doi.org/10.1080/00018732.2012.663070) (2012).
41. Parkin, S. S. P., Hayashi, M. & Thomas, L. Magnetic domain-wall racetrack memory. *Science* **320**, 190–194, DOI: [10.1126/science.1145799](https://doi.org/10.1126/science.1145799) (2008).
42. Romming, N. *et al.* Writing and Deleting Single Magnetic Skyrmions. *Science* **341**, 636–639, DOI: [10.1126/science.1240573](https://doi.org/10.1126/science.1240573) (2013).
43. Kim, T.-H. & Yeom, H. W. Topological Solitons versus Nonsolitic Phase Defects in a Quasi-One-Dimensional Charge-Density Wave. *Phys. Rev. Lett.* **109**, 246802, DOI: [10.1103/PhysRevLett.109.246802](https://doi.org/10.1103/PhysRevLett.109.246802) (2012).
44. Kim, T.-H., Cheon, S. & Yeom, H. W. Switching chiral solitons for algebraic operation of topological quaternary digits. *Nat. Phys.* **13**, 444–447, DOI: [10.1038/nphys4026](https://doi.org/10.1038/nphys4026) (2017).
45. Fincher, C. R., Chen, C. E., Heeger, A. J., MacDiarmid, A. G. & Hastings, J. B. Structural Determination of the Symmetry-Breaking Parameter in *trans* - (CH) x. *Phys. Rev. Lett.* **48**, 100–104, DOI: [10.1103/PhysRevLett.48.100](https://doi.org/10.1103/PhysRevLett.48.100) (1982).
46. Baeriswyl, D. & Maki, K. Soliton confinement in polyacetylene due to interchain coupling. *Phys. Rev. B* **28**, 2068–2073, DOI: [10.1103/PhysRevB.28.2068](https://doi.org/10.1103/PhysRevB.28.2068) (1983).
47. Baeriswyl, D. & Maki, K. Interchain order, soliton confinement, and electron-hole photogeneration in *trans* -polyacetylene. *Phys. Rev. B* **38**, 8135–8141, DOI: [10.1103/PhysRevB.38.8135](https://doi.org/10.1103/PhysRevB.38.8135) (1988).
48. Yeom, H. W. *et al.* Instability and Charge Density Wave of Metallic Quantum Chains on a Silicon Surface. *Phys. Rev. Lett.* **82**, 4898–4901, DOI: [10.1103/PhysRevLett.82.4898](https://doi.org/10.1103/PhysRevLett.82.4898) (1999).
49. Bunk, O. *et al.* Structure determination of the indium-induced si (111)-(4× 1) reconstruction by surface x-ray diffraction. *Phys. Rev. B* **59**, 12228 (1999).
50. Goldstone, J. & Wilczek, F. Fractional Quantum Numbers on Solitons. *Phys. Rev. Lett.* **47**, 986–989, DOI: [10.1103/PhysRevLett.47.986](https://doi.org/10.1103/PhysRevLett.47.986) (1981).
51. Heeger, A. J., Kivelson, S., Schrieffer, J. & Su, W.-P. Solitons in conducting polymers. *Rev. Mod. Phys.* **60**, 781 (1988).
52. Grüner, G. The dynamics of charge-density waves. *Rev. Mod. Phys.* **60**, 1129 (1988).
53. Ozawa, T. *et al.* Topological photonics. *Rev. Mod. Phys.* **91**, 015006 (2019).
54. Cooper, N., Dalibard, J. & Spielman, I. Topological bands for ultracold atoms. *Rev. Mod. Phys.* **91**, 015005 (2019).

Acknowledgements

We thank T.-H.K. for valuable discussions. C.-g.O., S.-H.H., and S.C. were supported by the National Research Foundation (NRF) of Korea through Basic Science Research Programs (NRF-2018R1C1B6007607 and NRF-2021R1H1A1013517), the research fund of Hanyang University (HY-2017), and the POSCO Science Fellowship of POSCO TJ Park Foundation.

Author contributions statement

S.C. conceived the project. C.-G.O and S.-H.H performed theoretical and numerical calculations under S.C. All authors discussed the results and co-wrote the manuscript.

Competing Interests

The authors declare no competing financial interests.

Additional information

Correspondence and requests for materials should be addressed to S.C.

Supplemental Information: Symmetry-Protected Solitons and Bulk-Boundary Correspondence in Generalized Jackiw-Rebbi Models

Chang-geun Oh,¹ Sang-Hoon Han,² and Sangmo Cheon^{1,2,3}

¹*Research Institute for Natural Sciences, Hanyang University, Seoul 04763, Korea*

²*Department of Physics, Hanyang University, Seoul 04763, Korea*

³*Institute for High Pressure, Hanyang University, Seoul, 04763, Korea*

CONTENTS

S1. Jackiw-Rebbi model	2
S1.1. Model	2
S1.2. Energy spectrum	2
S1.3. $\mathcal{T}, \mathcal{C}, \mathcal{P}$ symmetries	2
S1.4. Duality of JR solitons	2
S2. Generalized Jackiw-Rebbi model	3
S2.1. Model	3
S2.2. Energy spectrum	3
S2.2.1. Bulk spectrum	3
S2.2.2. Soliton modes	4
S2.2.3. Lorentz violation terms	4
S2.3. Fermion number	5
S2.4. Comparison with the tight-binding model	6
S2.5. $\mathcal{T}, \mathcal{C}, \mathcal{P}$ symmetries and dualities among solitons	6
S2.5.1. Bulk and NC soliton systems	6
S2.5.2. RC and LC soliton systems	6
S2.6. Field rotation symmetry	7
References	7

S1. JACKIW-REBBI MODEL

S1.1. Model

The Lagrangian density of the Jackiw-Rebba (JR) model [1, 2] with a complex fermion mass is given by

$$\mathcal{L}_{\text{JR}} = \bar{\psi}[i\gamma^0\partial_0 + i\gamma^1\partial_1 - \phi(x) - i\gamma^5 m_z]\psi, \quad (1)$$

where $\gamma^0 = \sigma^y$, $\gamma^1 = -i\sigma^z$, $\gamma^5 = \sigma^x$, m_z is a fermion mass, and $\phi(x)$ is a bose field in the double-well potential $V(\phi)$ that has two degenerate minima at $\phi = \pm\phi_0$. When $m_z = 0$, the Lagrangian density describes the low-energy effective theory of the Su-Schrieffer-Heeger (SSH) model [1–3]. When $m_z \neq 0$, the Lagrangian density describes the Rice-Mele (RM) model [4].

S1.2. Energy spectrum

The energy spectrum can be obtained by the one-particle Hamiltonian. For the homogeneous bose field in a minimum $\phi(x) = \phi_0$, the gapped energy spectrum of a JR model is given by $E = \pm\sqrt{k^2 + \phi_0^2 + m_z^2}$.

On the other hand, when the bose field is a soliton field [$\phi(x) = \phi_s(x)$] that varies spatially and connects the two degenerate minima [$\phi_s(\pm\infty) = \pm\phi_0$], there appears the isolated energy mode $E_s = m_z$ in the gap. For an anti-soliton field [$\phi(x) = \phi_{\bar{s}}(x) = -\phi_s(x)$], an isolated energy mode appears at $E_s = -m_z$. For the SSH model, all isolated energy mode are zero modes.

S1.3. $\mathcal{T}, \mathcal{C}, \mathcal{P}$ symmetries

For the SSH model, the Lagrangian density in Eq. (1) has $\mathcal{T}, \mathcal{C}, \mathcal{P}$ symmetries:

(i) Time reversal $t \rightarrow -t$

$$\mathcal{T}\psi(t, x)\mathcal{T}^{-1} = \gamma^5\gamma^0\psi(-t, x) \quad (2)$$

(ii) Charge conjugation

$$\mathcal{C}\psi(t, x)\mathcal{C}^{-1} = \psi^*(t, x) \quad (3)$$

(iii) Parity $x \rightarrow -x$

$$\mathcal{P}\psi(t, x)\mathcal{P}^{-1} = \gamma^0\psi(t, -x) \quad (4)$$

When the bose field is a soliton field, an additional parity transformation for the bose field $\mathcal{P}\phi_s(x)\mathcal{P}^{-1} = \phi_s(-x)$ should be accompanied. Therefore, the soliton system composed of $\psi_s(x)$ and $\phi_s(x)$ is self-charge conjugate [2].

For the RM model, \mathcal{C} and \mathcal{P} symmetries are broken due to the fermion mass m_z , while \mathcal{T} symmetry is preserved.

S1.4. Duality of JR solitons

We prove that a soliton system composed of $\psi_s(x)$ and $\phi_s(x)$ and the antisoliton system composed of $\psi_{\bar{s}}(x)$ and $\phi_{\bar{s}}(x)$ in the JR model form a charge conjugation and parity pair. That is, the charge conjugated field ($\psi_s^{\mathcal{C}}$) for a soliton system can be described with the help of the field ($\psi_{\bar{s}}$) in the antisoliton system and vice versa:

$$\psi_s^{\mathcal{C}} = \mathcal{C}\psi_s\mathcal{C}^{-1} = -\gamma^5\psi_{\bar{s}}^* \quad (5)$$

This can be proved by the equation of motion.

$$\text{e.o.m for soliton system: } [i\gamma^0(\partial_0 - ieA_0) + i\gamma^1(\partial_1 - ieA_1) - \phi_s - i\gamma^5 m_z]\psi_s = 0, \quad (6)$$

$$\text{e.o.m for charge conjugated soliton system: } [i\gamma^0(\partial_0 + ieA_0) + i\gamma^1(\partial_1 + ieA_1) - \phi_s - i\gamma^5 m_z]\psi_s^{\mathcal{C}} = 0, \quad (7)$$

$$\text{e.o.m for antisoliton system: } [i\gamma^0(\partial_0 - ieA_0) + i\gamma^1(\partial_1 - ieA_1) + \phi_s - i\gamma^5 m_z]\psi_{\bar{s}} = 0, \quad (8)$$

$$[i\gamma^0(\partial_0 + ieA_0) + i\gamma^1(\partial_1 + ieA_1) - \phi_s - i\gamma^5 m_z](\psi_{\bar{s}}^*) = 0. \quad (9)$$

From Eq. (8), one can obtain Eq. (9). Eq. (9) shows that $-\gamma^5\psi_{\bar{s}}^*$ satisfies the same equation of motion for charge conjugated soliton system in Eq. (7), which confirms Eq. (5).

Similarly, the parity transformed field for a soliton system can be described by the help of the field in an antisoliton system, and vice versa:

$$\mathcal{P}\psi_s(t, x)\mathcal{P}^{-1} = \gamma^0\gamma^5\psi_{\bar{s}}(t, -x), \quad (10)$$

$$\mathcal{P}\phi_s(x)\mathcal{P}^{-1} = \phi_s(-x) = \phi_{\bar{s}}(x). \quad (11)$$

S2. GENERALIZED JACKIW-REBBI MODEL

S2.1. Model

The Lagrangian density of the generalized JR model is

$$\mathcal{L} = \mathcal{L}_1 + \mathcal{L}_2 + \mathcal{L}_{\text{int}} + \mathcal{L}_B, \quad (12)$$

$$\mathcal{L}_j = \bar{\Psi}_j [i\partial\!\!\!/ - \Phi_j] \Psi_j, \quad (13)$$

$$\mathcal{L}_{\text{int}} = -\bar{\Psi}_1 [t_1 \gamma^0 - it_2 \gamma^1] \Psi_2 - \bar{\Psi}_2 [t_1 \gamma^0 + it_2 \gamma^1] \Psi_1, \quad (14)$$

$$\mathcal{L}_B = \frac{1}{2} (\partial_\mu \Phi_1 \partial^\mu \Phi_1 + \partial_\mu \Phi_2 \partial^\mu \Phi_2) - \frac{K}{2} (\Phi_1^2 + \Phi_2^2), \quad (15)$$

where Ψ_j and Φ_j are two-component spinor and real scalar bose fields ($j = 1, 2$). In this model, we minimally coupled two JR models by adding the inter-field coupling between Dirac fermion fields. Therefore, the potential for the Bose fields $U = -\frac{K}{2} (\Phi_1^2 + \Phi_2^2)$ has a $O(2)$ rotational symmetry. However, the total energy potential has a discrete symmetry (Z_2 or Z_4) depending on the interfield couplings, as discussed in the main text. For simplicity, we do not consider the possible interactions between bosons because we focus on the fermion fields and treat the bose fields as static background fields.

Using Clifford matrices, the Lagrangian density in Eq. (12) can be rewritten as follows:

$$\mathcal{L} = \bar{\Psi} [\Gamma_2 i\partial_0 + \Gamma_3 \partial_1 + t_1 \Gamma_{34} - it_2 \Gamma_{25} - \Phi] \Psi + \mathcal{L}_B, \quad (16)$$

where $\Psi = (\Psi_1, \Psi_2)$, $\Phi = \begin{pmatrix} \Phi_1 & 0 \\ 0 & \Phi_2 \end{pmatrix}$, $\bar{\Psi} = \Psi^\dagger \Gamma_2$. Here, Γ_a and Γ_{ab} ($a, b = 1, \dots, 5$) are gamma matrices. They are chosen as $\Gamma_a = (\sigma_z \otimes \tau_x, 1 \otimes \tau_y, 1 \otimes \tau_z, \sigma_x \otimes \tau_x, \sigma_y \otimes \tau_x)$, and $\Gamma_{ab} = \frac{1}{2i} [\Gamma_a, \Gamma_b]$.

S2.2. Energy spectrum

S2.2.1. Bulk spectrum

Here, we calculate the energy spectrum in a global minimum. From Eq. (16), we obtain 4×4 one-particle Hamiltonian. When the bose fields are in A or C minimum in Fig. 4(c), for instance, the one-particle Hamiltonian can be written as

$$H = \sigma_0 \otimes [k_x \tau_x \pm \Phi_0 \tau_y] + [t_1 \sigma_x \otimes \tau_0 + t_2 \sigma_y \otimes \tau_x], \quad (17)$$

where $+\Phi_0$ ($-\Phi_0$) is for A (C) minimum. The energy spectrum is given by which gives the following energy spectrum.

$$E = \pm \sqrt{\frac{A(\Phi_0, \Phi_0) \pm B(\Phi_0, \Phi_0)}{2}}, \quad (18)$$

$$A(\Phi_1, \Phi_2) = 2(k_x^2 + t_1^2 + t_2^2) + (\Phi_1^2 + \Phi_2^2), \quad (19)$$

$$B(\Phi_1, \Phi_2) = \sqrt{16(t_1^2 + t_2^2)k_x^2 + 4(t_1^2 + t_2^2)(\Phi_1^2 + \Phi_2^2) + 8(t_1^2 - t_2^2)\Phi_1\Phi_2 + (\Phi_1^2 - \Phi_2^2)^2}. \quad (20)$$

From this energy spectrum, we quickly check that the bands are degenerated when $t_1 = t_2 = 0$, while the bands are split when $t_1 \neq 0$ or $t_2 \neq 0$. Similarly, for the B and D minima, the same energy spectrum can be obtained except for the exchange between t_1 and t_2 .

The energy spectrum can also be calculated by using 2×2 effective one-particle Hamiltonian for each JR fields. From Eq. (12), we get the following equations of motion.

$$[i\partial\!\!\!/ - \Phi_1] \Psi_1 = [t_1 \gamma^0 - it_2 \gamma^1] \Psi_2, \quad [i\partial\!\!\!/ - \Phi_2] \Psi_2 = [t_1 \gamma^0 + it_2 \gamma^1] \Psi_1. \quad (21)$$

By inserting Eq. (21) into Eq. (12), the Lagrangian density of fermions can be described as two effective Lagrangian densities

$$\mathcal{L} = \mathcal{L}_1 + \mathcal{L}_2 + \mathcal{L}_{\text{int}} = \mathcal{L}_1^{\text{eff}} + \mathcal{L}_2^{\text{eff}}, \quad (22)$$

$$\mathcal{L}_j^{\text{eff}} = \bar{\Psi}_j [i\partial\!\!\!/ - \Phi_j] \Psi_j - \bar{\Psi}_j [t_1 \gamma^0 - (-1)^{j-1} it_2 \gamma^1] \frac{1}{i\partial\!\!\!/ - \Phi_j} [t_1 \gamma^0 + (-1)^{j-1} it_2 \gamma^1] \Psi_j. \quad (23)$$

For a constant or slowly-varying soliton bose field, the gradient of Φ_j is zero or very small. Then, the effective Lagrangian density in Eq. (23) can be approximated as

$$\mathcal{L}_j^{\text{eff}} \approx \bar{\Psi}_j [i\partial\!\!\!/ - \Phi_j] \Psi_j + \bar{\Psi}_j \left[t_1^2 \frac{i\gamma^0 \partial_0 - i\gamma^1 \partial_1 + \Phi_{3-j}}{\square + \Phi_{3-j}^2} + t_2^2 \frac{i\gamma^0 \partial_0 - i\gamma^1 \partial_1 - \Phi_{3-j}}{\square + \Phi_{3-j}^2} + (-1)^{j-1} 2t_1 t_2 \frac{i\gamma^5 \Phi_{3-j}}{\square + \Phi_{3-j}^2} \right] \Psi_j. \quad (24)$$

From each effective Lagrangian density in Eq. (24), the following effective one-particle Hamiltonian H_j for the positive frequency is obtained.

$$H_j = \left[-i\partial_x\sigma_x + \Phi_j\sigma_y + \frac{t_1^2 + t_2^2}{E^2 + \partial_x^2 - \Phi_{3-j}^2} (E - i\partial_x\sigma_x) + \frac{(t_1^2 - t_2^2)\Phi_{3-j}}{E^2 + \partial_x^2 - \Phi_{3-j}^2}\sigma_y + \frac{(-1)^{j-1}2t_1t_2\Phi_{3-j}}{E^2 + \partial_x^2 - \Phi_{3-j}^2}\sigma_z \right]. \quad (25)$$

By considering a plane-wave solution, the energy spectrum is given by $E = \pm\sqrt{\frac{A(\phi_1, \phi_2) \pm B(\phi_1, \phi_2)}{2}}$, which gives the same results in Eq. (18).

S2.2.2. Soliton modes

The isolated energy spectrum of the fermion field in the background soliton bose fields can be easily obtained with the effective Hamiltonians.

As an example, we consider the RC soliton system of which bose fields interpolate from A to B minima as shown in Fig. 2(d), $\Phi_1(\pm\infty) = \Phi_s(\pm\infty) = \mp\Phi_0$ and $\Phi_2(x) = \Phi_0$. Since the RC soliton can exist only at the critical point $t_1 = t_2$, the effective one-particle Hamiltonian in Eq. (25) becomes

$$H_j = \left[-i\partial_x\sigma_x + \Phi_j\sigma_y + \frac{2t_1^2}{E^2 + \partial_x^2 - \Phi_{3-j}^2} (E - i\partial_x\sigma_x) + \frac{(-1)^{j-1}2t_1^2\Phi_{3-j}}{E^2 + \partial_x^2 - \Phi_{3-j}^2}\sigma_z \right]. \quad (26)$$

As discussed in the main text, there are two isolated soliton modes. For an RC soliton system, the primary mode appears mainly in (Ψ_1, Φ_1) while the induced mode does in (Ψ_2, Φ_2) . Thus, H_1 and H_2 can be used to calculate the energy spectra of primary and induced modes, respectively.

We first calculate the spectrum of the primary mode. When $|x| \gg 1$, from Eq. (26), the energy eigenvalue equation for the primary mode can be approximated as

$$\left[-i\partial_x\sigma_x + \frac{E^2 - \Phi_0^2}{E^2 - \Phi_0^2 + 2t_1^2}\Phi_s(x)\sigma_y + \frac{2t_1^2}{E^2 - \Phi_0^2 + 2t_1^2}\Phi_0\sigma_z \right] \psi_P \approx E \frac{E^2 - \Phi_0^2 - 2t_1^2}{E^2 - \Phi_0^2 + 2t_1^2} \psi_P, \quad (27)$$

because the amplitude of the isolated soliton mode vanishes as it moves away from the soliton center.

By solving Eq.(27), the energy spectrum and wavefunction of the primary mode are given by

$$E_P = -\frac{2t_1^2}{\Phi_0} + O(t_1^4), \quad \psi_P \approx \begin{pmatrix} \exp[\int^x dx' \Delta_s(x')] \\ 0 \end{pmatrix}, \quad (28)$$

where $\Delta_s(x) = \frac{E_P^2 - \Phi_0^2}{E_P^2 - \Phi_0^2 + 2t_1^2}\Phi_s(x)$. Similarly, the energy spectrum of the induced mode can be obtained as $E_I = -\Phi_0 + t_1 - \frac{t_1^2}{4\Phi_0} + O(t_1^3)$ using H_2 , where one can also use a proper unitary transformation of $\psi_I \rightarrow \psi'_I = \frac{1}{\sqrt{2}}(1 - i\sigma_x)\psi_I$ for convenience. In the same way, the energy spectra of soliton modes in LC soliton systems can be obtained.

For NC soliton systems, the energy spectra of the hybridized bonding and antibonding soliton modes can also be calculated regardless of t_1 and t_2 in a similar way. For a more straightforward calculation, one can use the hybridized bonding and antibonding fields. For instance, $\Psi_B = \frac{1}{\sqrt{2}}[\Psi_1 - \Psi_2]$ and $\Psi_{AB} = \frac{1}{\sqrt{2}}[\Psi_1 + \Psi_2]$ can be used in the NC soliton system of which bose fields interpolate from A to C minima. The calculated spectra are plotted in Fig. 3 for $t_1 = t_2$ case and in Fig. S1 for $t_1 \neq t_2$ case.

S2.2.3. Lorentz violation terms

Here, we discuss the Lorentz violating terms in the effective Lagrangian density and their effects on the spectra of the soliton modes. When $t_1 = t_2$, from Eq. (24), the effective Lagrangian density for the j th field is given by

$$\mathcal{L}_j^{\text{eff}} = \bar{\Psi}_j [i\cancel{\partial} - \Phi_j] \Psi_j + \bar{\Psi}_j \left[\frac{2t_1^2 i\gamma^0 \partial_0 - i\gamma^1 \partial_1 + (-1)^{j-1} i\gamma^5 \Phi_{3-j}}{\square + \Phi_{3-j}^2} \right] \Psi_j. \quad (29)$$

This effective Lagrangian has two types of Lorentz violating terms: A chiral mass term which is proportional to $2t_1^2\Phi_{3-j}\gamma^5$ and two space-time deformation terms which are proportional to $2t_1^2\gamma^1$ and $2t_1^2\gamma^0$, respectively. Even though both can give corrections to the physical quantities, the space-time deformation terms give higher-order corrections and hence can be ignored in the leading order. For example, consider the energy spectrum of the primary mode in an RC soliton system. If we calculate the energy spectrum ignoring the space-time deformation terms, we have $E_P = -\frac{2t_1^2}{\Phi_0} + O(t_1^4)$, which gives the same result with Eq. (28) up to t_1^3 order.

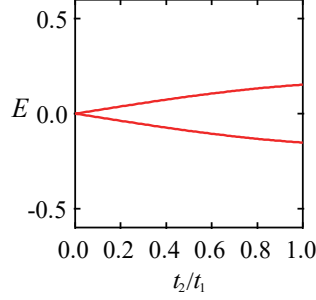


Fig. S1. Energy spectra for bonding and antibonding modes in an NC soliton system with respect to t_2/t_1 . The upper and lower lines represent the energy spectra for antibonding and bonding modes, respectively. The spectra are normalized by the energy gap. Here, $t_1 = 0.1$. When $t_2/t_1 = 0$, bonding and antibonding become two degenerate zero modes even in the presence of the interfield coupling, which is consistent with the ladder-SSH model [5].

S2.3. Fermion number

The zero mode in the SSH model has the quantized $\frac{1}{2}$ fermion number [1, 3]. Similarly, the isolated soliton modes in the generalized JR model have fractional fermion numbers. We calculate the fermion number of each isolated soliton mode using the Goldstone-Wilczek method [6] and effective Lagrangian densities.

As an example, we calculate the fractional fermion number of the isolated modes in the RC soliton system of which bose fields interpolate from A to B minima, i.e, $\Phi_1(\pm\infty) = \Phi_s(\pm\infty) = \mp\Phi_0$ and $\Phi_2(x) = \Phi_0$. First, we consider the fermion number of the primary mode, which mainly exists in Ψ_1 . From Eq. (29), the effective Lagrangian density for Ψ_1 can be approximated as

$$\mathcal{L}_1^{\text{eff}} \approx \bar{\Psi}_1 [i\partial\!\!\!/ - (\Phi_s - i\gamma^5 \frac{2t_1^2\Phi_0}{\Phi_0^2 - E^2})] \Psi_1. \quad (30)$$

Here, up to leading order, we ignore space-time deformations because they give the higher order correction similar to the energy spectrum as we discussed in S2.2.3.

Note that E^2 in Eq. (30) has two degrees of freedom because there are two occupied bands in the energy spectrum in Eq. (18): $E_+^2 = \frac{A(\Phi_1, \Phi_2) + B(\Phi_1, \Phi_2)}{2}$, $E_-^2 = \frac{A(\Phi_1, \Phi_2) - B(\Phi_1, \Phi_2)}{2}$. Then, the induced current $\langle j_{E_{\pm}}^{\mu}(x) \rangle$ and the fermion number $Q(E_{\pm})$ for each bands E_{\pm} are given by

$$\langle j_{E_{\pm}}^{\mu}(x) \rangle = -\frac{1}{2\pi} \epsilon^{\mu\nu} \partial_{\nu} \theta, \quad (31)$$

$$Q(E_{\pm}) = \int dx j_{E_{\pm}}^{\mu}(x), \quad (32)$$

where

$$\tan\theta \equiv -\frac{2t_1^2\Phi_0}{(\Phi_0^2 - E_{\pm}^2)\Phi_s(x)}. \quad (33)$$

Hence, the fermion number of the primary mode is given by

$$Q_P^{\text{RC}} = \frac{1}{2}Q(E_+) + \frac{1}{2}Q(E_-), \quad (34)$$

$$= -\frac{1}{2\pi} \left[\tan^{-1} \frac{2t_1^2}{\Phi_0^2 - E_+^2} + \tan^{-1} \frac{2t_1^2}{\Phi_0^2 - E_-^2} \right]. \quad (35)$$

Here, $\frac{1}{2}$ is a factor for the total fermion number conservation between zero interfield coupling case ($t_1 = 0$) and nontrivial interfield coupling case ($t_1 \neq 0$). When $t_1 = 0$, the primary mode in the RC soliton system is reduced to the zero mode in the SSH model, which has a fractional fermion number $-\frac{1}{2}$. Hence, using the properties of tangent function, the fermion number in Eq. (34) is modified to

$$Q_P^{\text{RC}} = -\frac{1}{2\pi} \left[\tan^{-1} \frac{2t_1^2}{\Phi_0^2 - E_+^2} + \tan^{-1} \frac{2t_1^2}{\Phi_0^2 - E_-^2} \right] - \frac{1}{2}. \quad (36)$$

Similarly, the fermion number of the induced mode which mainly resides in Ψ_2 can be obtained as below:

$$Q_I^{\text{RC}} = \frac{1}{2\pi} \left[\tan^{-1} \frac{2t_1^2}{\Phi_0^2 - E_+^2} + \tan^{-1} \frac{2t_1^2}{\Phi_0^2 - E_-^2} \right]. \quad (37)$$

Note that the total fermion number of primary and induced modes in an RC soliton system is always quantized as $Q_P^{\text{RC}} + Q_I^{\text{RC}} = -1/2$ regardless of the strength of t_1 .

Using a similar method, the fermion numbers of soliton modes for LC and NC soliton systems can be calculated. The final results are summarized as follows:

$$Q_P^{\text{RC}} = -x - 1/2, \quad Q_I^{\text{RC}} = +x, \quad (38)$$

$$Q_P^{\text{LC}} = +x - 1/2, \quad Q_I^{\text{LC}} = -x, \quad (39)$$

$$Q_{\text{AB}}^{\text{NC}} = -1/2, \quad Q_{\text{B}}^{\text{NC}} = -1/2, \quad (40)$$

where $x = \frac{1}{2\pi} \left[\tan^{-1} \frac{2t_1^2}{\Phi_0^2 - E_+^2} + \tan^{-1} \frac{2t_1^2}{\Phi_0^2 - E_-^2} \right]$. The opposite signs of x between RC and LC soliton systems indicate that RC and LC solitons form a charge conjugation pair. For an NC soliton system, each fermion number of bonding and antibonding modes is $-1/2$ regardless of t_1 and t_2 values.

S2.4. Comparison with the tight-binding model

We compare the analytically obtained energy spectra and charges of the isolated soliton modes with numerically calculated results at $t_1 = t_2$ case. The numerical calculations were performed using the tight-binding method for the double Peierls chain model [7]. The charge is calculated from the difference of Berry phases between the two global minima because the difference of Berry phases is proportional to the topological charge of a soliton that interpolates the same two global minima[8, 9]. Both results fit well with each other, as shown in Fig. 3(d-i).

S2.5. $\mathcal{T}, \mathcal{C}, \mathcal{P}$ symmetries and dualities among solitons

S2.5.1. Bulk and NC soliton systems

The system has $\mathcal{T}, \mathcal{C}, \mathcal{P}$ symmetries when the bose fields are localized in the AC or BD lines in Fig. 4(c) of the main text. When the bose fields are localized in the AC line, the system has the following symmetries:

$$\mathcal{T}\Psi(t, x)\mathcal{T}^{-1} = \Gamma_3\Psi(-t, x), \quad (41)$$

$$\mathcal{C}\Psi(t, x)\mathcal{C}^{-1} = -\Gamma_{14}\Psi^*(t, x), \quad (42)$$

$$\mathcal{P}\Psi(t, x)\mathcal{P}^{-1} = \Gamma_{34}\Psi(t, -x), \quad (43)$$

$$\mathcal{P}\Phi(x)\mathcal{P}^{-1} = \Phi(-x). \quad (44)$$

When the bose fields are in the BD line, the system has the following symmetries:

$$\mathcal{T}\Psi(t, x)\mathcal{T}^{-1} = \Gamma_3\Psi(-t, x), \quad (45)$$

$$\mathcal{C}\Psi(t, x)\mathcal{C}^{-1} = -\Gamma_5\Psi^*(t, x), \quad (46)$$

$$\mathcal{P}\Psi(t, x)\mathcal{P}^{-1} = \Gamma_{24}\Psi(t, -x), \quad (47)$$

$$\mathcal{P}\Phi(x)\mathcal{P}^{-1} = \Phi(-x). \quad (48)$$

Hence, the global minima have $\mathcal{T}, \mathcal{C}, \mathcal{P}$ symmetries. Likewise, NC soliton systems that are localized in either AC or BD lines have $\mathcal{T}, \mathcal{C}, \mathcal{P}$ symmetries, which leads that an NC soliton is its own anti-NC soliton.

S2.5.2. RC and LC soliton systems

RC and LC soliton systems have the same \mathcal{T} symmetry:

$$\mathcal{T}\Psi(t, x)\mathcal{T}^{-1} = \Gamma_3\Psi(-t, x). \quad (49)$$

On the other hand, \mathcal{C} and \mathcal{P} symmetries are broken. The broken \mathcal{P} symmetry indicates that RC and LC solitons have chiralities.

The charge conjugated and parity transformed fields for an RC soliton system can be described by the help of the field in an LC soliton system and vice versa.

$$\mathcal{C}\Psi_{\text{RC}(i \rightarrow j)}(t, x)\mathcal{C}^{-1} = -\Gamma_{14}U\Psi_{\text{LC}(j \rightarrow i)}^*(t, x), \quad (50)$$

$$\mathcal{P}\Psi_{\text{RC}(i \rightarrow j)}(t, x)\mathcal{P}^{-1} = \Gamma_{34}U^*\Psi_{\text{LC}(j \rightarrow i)}(t, -x), \quad \mathcal{P}\Phi(x)\mathcal{P}^{-1} = \Phi(-x), \quad (51)$$

where i and j in the subscript indicate two global minima that the corresponding soliton field connects. And the unitary matrices U are given by

$$U = \begin{pmatrix} 0 & 1 \\ -i\sigma_x & 0 \end{pmatrix}, \quad \text{when } (i, j) = (A, B) \text{ or } (C, D),$$

$$U = \begin{pmatrix} 0 & i\sigma_x \\ 1 & 0 \end{pmatrix}, \quad \text{when } (i, j) = (B, C) \text{ or } (D, A).$$

This indicates RC and LC solitons form a particle-antiparticle and chiral pair. One can check such particle-antiparticle duality using equations of motion including $U(1)$ electromagnetic fields. For example, we consider the RC and LC soliton systems with $(i, j) = (A, B)$. Then, the fermion field $\Psi_{\text{RC}(A \rightarrow B)}(t, x)$ satisfies the following equation of motion:

$$[(i\partial_0 - eA_0)\Gamma_2 + (\partial_1 + ieA_1)\Gamma_3 + t_1\Gamma_{34} - it_2\Gamma_{25} + \Phi_s(x)A + \Phi_0B]\Psi_{\text{RC}(A \rightarrow B)}(t, x) = 0. \quad (52)$$

The charge conjugated field $\Psi_{\text{RC}(A \rightarrow B)}^{\mathcal{C}}(t, x)$ satisfies

$$[(i\partial_0 + eA_0)\Gamma_2 + (\partial_1 - ieA_1)\Gamma_3 + t_1\Gamma_{34} - it_2\Gamma_{25} + \Phi_s(x)A + \Phi_0B]\Psi_{\text{RC}(A \rightarrow B)}^{\mathcal{C}}(t, x) = 0. \quad (53)$$

The fermion field $\Psi_{\text{LC}(B \rightarrow A)}(t, x)$ in the LC soliton system satisfies

$$[(i\partial_0 - eA_0)\Gamma_2 + (\partial_1 + ieA_1)\Gamma_3 + t_1\Gamma_{34} - it_2\Gamma_{25} - \Phi_s(x)A + \Phi_0B]\Psi_{\text{LC}(B \rightarrow A)}(t, x) = 0. \quad (54)$$

If we take $\Gamma_{14}U^*$ after applying the complex conjugation to Eq. (54), we get

$$[(i\partial_0 + eA_0)\Gamma_2 + (\partial_1 - ieA_1)\Gamma_3 + t_1\Gamma_{34} - it_2\Gamma_{25} + \Phi_s(x)A + \Phi_0B](\Gamma_{14}U^*)\Psi_{\text{LC}(B \rightarrow A)}(t, x) = 0. \quad (55)$$

From Eq. (55), one can see that $(\Gamma_{14}U^*)\Psi_{\text{LC}(B \rightarrow A)}(t, x)$ satisfies the same equation of motion for the charge conjugated field of an RC soliton system in Eq. (53), which implies Eq. (50). Similarly, the chiral duality between RC and LC solitons can be checked.

S2.6. Field rotation symmetry

Two rotational transformations can be considered in the generalized JR model: π -rotation ($n = 2$) and $\pi/2$ -rotation ($n = 1$). The rotation is given by

$$\Psi(t, x) \rightarrow \begin{pmatrix} 0 & -i\sigma_x \\ 1 & 0 \end{pmatrix}^n \Psi(t, x), \quad (56)$$

$$\Phi(x) \rightarrow e^{i\Gamma_{14}\theta}\Phi(x), \quad (57)$$

where $e^{i\Gamma_{14}\theta} = \begin{pmatrix} \cos \theta & \sin \theta \\ -\sin \theta & \cos \theta \end{pmatrix}$ and $\theta = \frac{n\pi}{2}$. If we take the $\pi/2$ -rotation, t_1 and t_2 are exchanged. Hence, the Lagrangian density is invariant under the $\pi/2$ -rotation only when $t_1 = t_2$. Under the π -rotation, t_1 and t_2 exchange twice, which implies that the Lagrangian density is invariant regardless of t_1 and t_2 values.

-
- [1] R. Jackiw and J. Schrieffer, Nuclear Physics B **190**, 253 (1981).
 - [2] R. Jackiw and C. Rebbi, Phys. Rev. D **13**, 3398 (1976).
 - [3] W. P. Su, J. R. Schrieffer, and A. J. Heeger, Phys. Rev. Lett. **42**, 1698 (1979).
 - [4] M. J. Rice and E. J. Mele, Phys. Rev. Lett. **49**, 1455 (1982).
 - [5] D. Baeriswyl and K. Maki, Phys. Rev. B **28**, 2068 (1983).
 - [6] J. Goldstone and F. Wilczek, Phys. Rev. Lett. **47**, 986 (1981).
 - [7] S. Cheon, T.-H. Kim, S.-H. Lee, and H. W. Yeom, Science **350**, 182 (2015).
 - [8] X.-L. Qi, T. L. Hughes, and S.-C. Zhang, Phys. Rev. B **78**, 195424 (2008).
 - [9] C.-g. Oh, S.-H. Han, S.-G. Jeong, T.-H. Kim, and S. Cheon, Sci Rep **11**, 1013 (2021).